Capillary effects in a confined smectic phase of hard spherocylinders: Influence of particle elongation

D. de las Heras

Departamento de Física Teórica de la Materia Condensada, Universidad Autónoma de Madrid, E-28049 Madrid, Spain

E. Velasco

*Departamento de Física Teórica de la Materia Condensada and Instituto de Ciencia de Materiales Nicolás Cabrera,
Universidad Autónoma de Madrid, E-28049 Madrid, Spain*

L. Mederos

Instituto de Ciencia de Materiales, Consejo Superior de Investigaciones Científicas, E-28049 Cantoblanco, Madrid, Spain
(Received 25 April 2006; published 24 July 2006)

A system of hard rods confined into a pore with slit geometry (two parallel planar substrates) is studied theoretically in the regime of high packing fraction. In this regime the bulk system exhibits a nematic phase as well as a smectic-*A* (spatially layered) phase. When the system is confined, strong commensuration effects between the layer spacing and the pore width bring about a rich phenomenology, with a phase diagram showing layering and capillary transitions. The latter include capillary smectization transitions whereby a confined smectic phase occurs at conditions of saturation different from those of the corresponding bulk fluid. These transitions are seen to be intimately connected with layering transitions involving discontinuous changes in the number of layers inside the pore. This rich phenomenology is obtained by use of a sophisticated density-functional, Onsager-theory-based approach, especially suited to deal with strongly inhomogeneous fluids. The theory allows for a unified description of ordering and phase behavior of the fluid in confined geometry, and permits us to correlate the above behavior with the wetting properties of the fluid on a single substrate.

I. INTRODUCTION

Surface and interfacial properties of liquid crystals have attracted considerable interest since these materials were discovered [1,2]. From a practical or technological point of view, surface properties and surface phase transitions are of crucial importance, since they in part determine the macroscopic behavior of the materials and, as a consequence, their suitability for practical uses, the more extended being the manufacture of display devices [3]. From a purely theoretical point of view liquid crystals and, particularly, liquid crystals in a confined geometry, pose formidable challenges because of their structural complexity (molecular interactions are largely unknown) and orientational degrees of freedom [4]. The latter, which are coupled to translational degrees of freedom, are the origin of their peculiar properties, midway between the isotropic liquid and the crystal but, at the same time, are the origin of the great difficulties involved in the formulation of theoretical models. As a consequence, microscopic models of liquid crystals and their surface properties must still be considered as toy models. Nevertheless, these are relevant because their simplified nature forces us to focus attention on the relevant aspects that account, at least qualitatively, for the particular phenomenology of liquid crystals. These aspects include particle elongation, particle overall shape, and so on.

When a liquid crystal is placed in front of a surface, a competition between the intrinsic (liquid crystal particles) and extrinsic (liquid crystal particles and substrate) interactions is established. The result is, in general, a very rich surface phenomenology, which includes surface phase transitions such as wetting, anchoring, and coupling between the two [1]. Confinement of the material into a narrow pore causes remarkable capillary effects [5], which find interesting applications. Most theoretical [6] and simulation [7–9] studies have focused on nematic fluids, while smectic films or films with presmectic order have received little theoretical attention [10–12], while experimental studies are scarce [13–16]. The effect of confinement on smectic films is even more dramatic than in nematic films because of the commensuration effects between the characteristic length scale (particle elongation) of the fluid and the imposed length scale (pore width). Commensuration effects are expected to be significant in cases where the system is in a thermodynamic state close to that which would correspond to a spatially ordered (smectic) phase in bulk. The result is the existence of remarkable capillary effects in liquid crystals confined in narrow pores, conceptually similar to well-known capillary effects in confined simple liquids, such as the phenomenon of capillary condensation [17] and layering and capillary crystallization [18,19].

The first theoretical investigations on confined liquid crystals were conducted by Sheng [20], and Poniewierki and Sluckin [21] who predicted what can be termed *capillary nematization*. They suggested that the nematic-isotropic transition temperature of a liquid crystal confined between two parallel walls may be larger or smaller than the corresponding value for the bulk nematic-isotropic transition as the distance between the walls decreases, the wetting conditions prevailing at the walls being the relevant factor. The predicted capillary nematization has recently been observed, using atomic force microscopy, by Kocevar *et al.* [22] on a

thermotropic nematic liquid crystal; the associated first-order transition line, terminated in a critical point, was also observed. A microscopic toy model that accounts for this phenomenology has recently been presented [23]. In this model liquid crystals particles are represented by hard spherocylinders while the effects of the pore walls are introduced by means of an external potential acting on each spherocylinder. An extended Onsager density-functional theory is then used to obtain the thermodynamic properties of the system.

Our main goal in this paper is to extend our previous study [24] to include the effect of particle elongation. In previous work we presented an extension of the molecular toy model mentioned above to account for capillary effects in a liquid crystal confined into a narrow slitlike pore, an extension which is particularly suitable for dealing with the strong oscillatory behavior in the local density characteristic of positionally ordered phases, such as the smectic phase and/or confined liquid crystals. For some particular aspect ratio of the particles, we found interesting commensuration effects and a complete phase diagram including both layering and capillary smectization lines; these results are conceptually similar to those found in other physical systems [25–27], but our work somehow permitted a unified description of all phenomenologies. In the present paper we analyze how these effects change as the particle shape is varied. The rest of the paper is arranged as follows. In the following section, Sec. II, the model is summarized. In Sec. III we present the results, paying particular attention to the role of the particle aspect ratio in the behavior of the confined fluid. Finally, some conclusions are drawn in Sec. IV. Some details of the density functional and its numerical implementation are given in the Appendix.

II. THEORETICAL MODEL

Virtually all theoretical treatments of fluids made of anisotropic hard-core particles start from Onsager theory [28] or variations. As applied to a system of hard spherocylinders (HSCs), Onsager theory predicts an isotropic to nematic transition at some particular density, a prediction that becomes exact in the limit of infinitely long hard rods. The theory is a second-order virial expansion, hence a density-functional theory (DFT) (based on the one-particle orientational distribution function), and has been extended, using the so-called decoupling approximation [29], to include higher-order virial coefficients in an approximate way, allowing for more accurate results to be obtained for realistic molecular models (i.e., finite aspect ratio of the particles).

A few attempts have been made to extend Onsager ideas to general inhomogeneous systems (see, e.g., Refs. [30–32]) and nonuniform systems (such as the bulk smectic phase) in particular [33]. In this section we shall summarize the extended Onsager approximation used in our calculation, which is appropriate to deal with highly inhomogeneous fluids and has been applied successfully several times (see, e.g., Refs. [33,34]). We present only a brief sketch of the theory. Details on the theory and on the numerical implementation can be found in the Appendix; further description of the model can be found elsewhere [33].

We consider a fluid confined into a slitlike pore, with confining walls parallel to the xy plane and separated by a distance H. The normal to the walls is along the z axis. The free-energy functional $F[\rho]$ is expressed, as usual, as the sum of ideal $F_{id}[\rho]$ and excess $F_{ex}[\rho]$ contributions. The ideal part is exactly given by the following functional:

$$F_{id}[\rho] = kT \int \int d\mathbf{r} d\mathbf{\Omega} \rho(\mathbf{r},\mathbf{\Omega})\{\ln[\Lambda^3\rho(\mathbf{r},\mathbf{\Omega})] - 1\}, \quad (1)$$

where $\rho(\mathbf{r},\mathbf{\Omega})$ is the one-particle distribution function, which gives the mean local density of uniaxial particles at $\mathbf{r}$ and with orientation of their symmetry axes given by $\mathbf{\Omega} \equiv (\theta,\phi)$, k is the Boltzmann's constant, T is the temperature, and Λ is the thermal wavelength. The excess part is written as

$$F_{ex}[\rho] = \int d\mathbf{r} \frac{\Psi_{ex}^{PHE}[\bar{\rho}(\mathbf{r})]}{\bar{\rho}_{PHE}(\mathbf{r})} \int d\mathbf{\Omega}\rho(\mathbf{r},\mathbf{\Omega})$$
$$\times \int \int d\mathbf{r}' d\mathbf{\Omega}' \rho(\mathbf{r}',\mathbf{\Omega}')V_{exc}(\mathbf{r}-\mathbf{r}',\mathbf{\Omega},\mathbf{\Omega}'), \quad (2)$$

where $\bar{\rho}(\mathbf{r})$ and $\bar{\rho}_{PHE}(\mathbf{r})$ are averaged densities, details of which are given in the Appendix. This can also be viewed as a particular implementation of density-functional theory (due to Somoza and Tarazona [34]) that generalizes Parsons-Lee theory to highly nonuniform liquid-crystalline phases. The theory is based on the weighted-density approximation (WDA) for simple fluids made of isotropic particles [35]. The one-particle distribution function can be written as $\rho(\mathbf{r},\mathbf{\Omega}) \equiv \rho(z,\mathbf{\Omega}) = \rho(z)f(z,\mathbf{\Omega})$ where $\rho(z)$, the density profile, is now the mean number of particles at z, regardless of their orientation, and $f(z,\mathbf{\Omega})$ is the orientational distribution function. Note that we have made use of the particular symmetry of our system since only the spatial dependence on z, the distance perpendicular to the pore wall, is relevant.

For axially symmetric particles (with spatial dependence only along the z direction) the following parametrization of the orientational distribution function is useful:

$$f(z,\theta) = \frac{e^{\Lambda(z)P_2(\cos\theta)}}{\int d\mathbf{\Omega}e^{\Lambda(z)P_2(\cos\theta)}}. \quad (3)$$

The orientational order parameter η is defined in the usual manner:

$$\eta(z) = \int d\mathbf{\Omega}P_2(\cos\theta)f(z,\theta). \quad (4)$$

It turns out that the fluid can be uniquely described by the density $\rho(z)$ and order-parameter $\eta(z)$ profiles (see the Appendix). In order to end the description of our density-functional model we have to specify the extrinsic contribution to the free energy, i.e., the contribution coming from the interaction of the liquid crystal molecules with the pore walls. This is given by

$$F_w[\rho] = \int \int d\mathbf{r} d\hat{\mathbf{\Omega}} \rho(\mathbf{r}, \hat{\mathbf{\Omega}}) V_w(z), \qquad (5)$$

where the external potential $V_w(z)$ is such that

$$e^{-\beta V_w(z)} = \Theta(z) + \Theta(H - z) \qquad (6)$$

where $\beta = 1/kT$, and $\Theta(x)$ is the Heaviside function. As shown in Ref. [23] this potential, which represents two hard walls acting on the centres of mass of the particles, induces homeotropic alignment in a monolayer of spherocylinders adsorbed on a single wall. Thus it will induce homeotropic alignment and therefore a director configuration perpendicular to the two (identical) walls in the confined system. In particular, the layers of the confined smectic phase will arrange themselves parallel to the walls.

Since we are dealing with a confined systems, the equilibrium configuration is obtained by minimizing the grand potential functional, given by

$$\Omega[\rho] = F_{id}[\rho] + F_{ex}[\rho] + F_w[\rho] - \mu \int \int d\mathbf{r} d\hat{\mathbf{\Omega}} \rho(\mathbf{r}, \hat{\mathbf{\Omega}}),$$
$$(7)$$

where μ is the chemical potential of the system. For a given pore width H and chemical potential μ, the grand potential $\Omega([\rho]; \mu, H)$ is minimized with respect to $\rho(z)$ and $\eta(z)$ using a standard conjugate-gradient method. Details on this procedure are given in the Appendix.

III. RESULTS: STRUCTURE AND PHASE DIAGRAMS

In this section we present and describe our results for the structure (density and orientational distributions) and phase behavior of the system. We have focused attention on confined hard-spherocylinder systems of length-to-breadth ratios $L/D = 3.7$, 5, and 6. In the first case, $L/D = 3.7$, the system is below the bulk isotropic-nematic-smectic-A (INS) triple point as predicted by the same approximation when applied to the bulk system, and therefore the nematic phase is not thermodynamically stable. Although we have not calculated the precise location of the triple point, the bulk IS transition takes places at a pressure lower than that corresponding to the IN bulk transition. The contrary situation holds for $L/D = 4$, which indicates that $3.7 < (L/D)_{INS} < 4$. This result is in agreement with previous calculations of ours based on the same model (but with a slightly different numerical approach, see Ref. [33]), and also with computer simulations [36,37]. Therefore for elongation $L/D = 3.7$, the smectic phase coexists with the isotropic phase. In the two other cases considered, $L/D = 5$ and 6, the nematic phase is thermodynamically stable, and the smectic phase coexists with the nematic phase.

In Fig. 1 density profiles of different confined structures are shown. The profiles result from a minimization of the density functional with different conditions of chemical potential and pore width (note that in each case only half of the profile is shown, since the profiles are symmetric with respect to a plane at the center of the pore and parallel to the walls). The profile in Fig. 1(a) corresponds to a structure
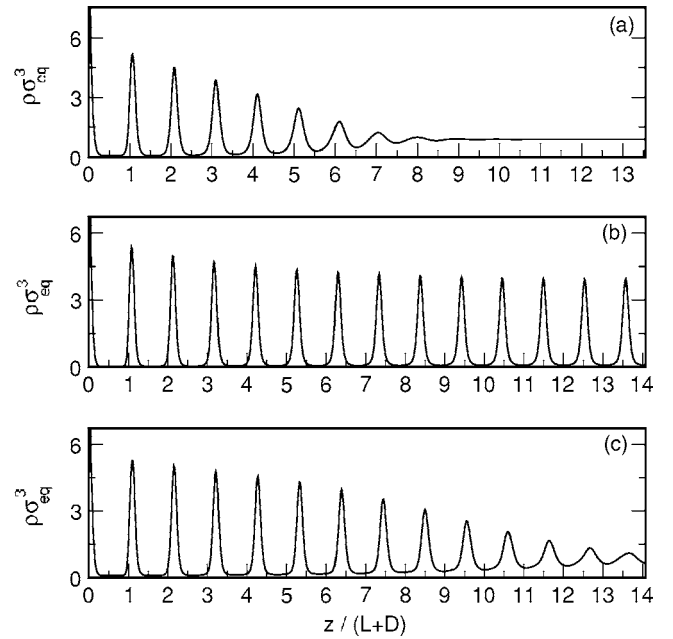

FIG. 1. Density profiles for the following cases: (a) $L/D = 3.7$, $\mu = \mu_{IS}^{coex} - 0.13kT$, and $H = 27.1(L+D)$; (b) $L/D = 6.0$, $\mu = \mu_{NS}^{coex} + 0.51kT$ and $H = 28.2(L+D)$; and (c) $L/D = 6.0$, $\mu = \mu_{NS}^{coex} + 0.51kT$ and $H = 28.2(L+D)$. Values for the coexistence chemical potentials are given in Table I. Profiles in (b) and (c) correspond to two structures that coexist in thermodynamic equilibrium. Note that the vertical scale is too short to accommodate the density profiles in the region immediately next to the wall.

with no positional order in the central region of the pore; the orientational profile (not shown) is zero in this region. We can term this phase "isotropic" (I), since the central region exhibits properties of a bulk isotropic phase. The profiles in Figs. 1(b) and 1(c) correspond to two structures with the same pore width that coexist in thermodynamic equilibrium (i.e., equal grand potentials). No continuous path exists in the variables μ-H (chemical potential–pore width) connecting these profiles. Since the first has well defined layers, we can call it confined "smectic" (S_n, meaning that the phase has n smectic periods, i.e., $n+1$ smectic layers). The other profile [Fig. 1(c)] is also well structured, but both the density and orientational profiles in the central region of the pore show damped oscillations; this we call confined "nematic" (N) phase (in the following, when the distinction between I and N phases does not need to be made, we will use D to denote collectively these two "disordered" phases). However, as usual in confined fluids, the distinction between confined nematic, smectic, or even isotropic phases is not clearcut, and a simple inspection of the profiles may not provide a definite conclusion as to the nature of the confined phase. This nature is to be ascribed according to the topology of the phase diagram. Note that all profiles show strongly varying peaks next to the walls. The associated oscillations die out from the wall but, in most instances, they clearly reach the central region.

Figure 2 shows schematically the phase diagrams obtained for the three particle elongations considered, in the plane μ-H. First-order transition lines are drawn with con-
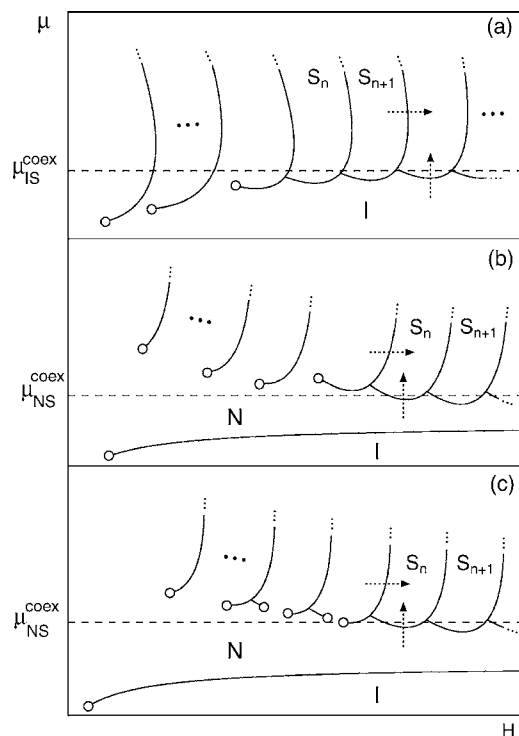
FIG. 2. Schematic representation of the effect of particle length-to-breadth ratio L/D on the phase diagram of the confined liquid crystal. μ is the chemical potential and H is the pore width. (a) $L/D=3.7$; (b) $L/D=5$; and (c) $L/D=6$. Dashed horizontal line indicates bulk transition to smectic phase. Arrows indicate particular paths in the phase diagram connecting two confined phases (see text for a detailed discussion). Labels approximately indicate regions where confined isotropic (I), nematic (N), and smectic (S) phases are stable. In the latter case the subscript n gives the number of layers of the smectic structure. Although not apparent in the figure, the three lines meeting at triple points should do so with different slopes.

tinuous lines, while circles represent critical points. The figure represents the basic topology of the phase diagrams, based on real data. The latter have been obtained by minimization of the density functional and by locating the phase boundaries in the usual way (i.e., searching for equality of excess grand potentials of the different phases involved). Later we present actual results for particular values of pore width.

The first apparent difference among these phase diagrams is that the IN transition line does not appear in the case of $L/D=3.7$, consistent with the fact, commented above, that this system is below the bulk INS triple point and therefore a direct IS transition takes place with increasing chemical potential. In the two other cases, a *capillary nematization* line, corresponding to the IN transition in the confined material, is present. Confinement promotes nematic order so that for finite H the IN transition takes place at values of the chemical potential different from that of the bulk IN transition. The $\mu_{IN}(H)$ transition line is monotonically increasing in both cases: as H increases the nematization line asymptotically tends to the bulk IN transition so that the nematization line becomes horizontal for large values of H. This trend is governed by the (macroscopic) Kelvin equation,

$$\mu_{IN}(H) - \mu_{IN}^{coex} = \frac{2(\gamma_{WN} - \gamma_{WI})}{(\rho_N - \rho_I)H}, \quad H \to \infty \quad (8)$$

which relates the difference in chemical potential between the capillary nematization line $\mu_{IN}(H)$ and the bulk value $\mu_{IN}^{coex} = \mu_{IN}(H \to \infty)$ with the values of the surface tensions of the wall-nematic interface γ_{WN} and wall-isotropic interface γ_{WI} and with the densities of the nematic and isotropic phases at bulk coexistence, ρ_N and ρ_I, respectively. Since $\rho_N > \rho_I$ always, the fact that the slope $d\mu_{IN}(H)/dH > 0$, as seen in the graphs, means that the wall is preferentially wet by the nematic phase over the isotropic phase, i.e., $\gamma_{WN} < \gamma_{WI}$. This is actually the case since, in the two cases $L/D=5$ and 6, we find that there is complete wetting of the wall by the nematic phase [31], so that $\gamma_{WN} + \gamma_{IN} = \gamma_{WI}$; since $\gamma_{IN} > 0$ this means $\gamma_{WN} < \gamma_{WI}$. For narrow enough pores, the capillary nematization line ends in a critical point below which no IN transition is found. The existence of the critical point can be qualitatively understood in terms of how the order parameter varies in the pore: when H is small enough, the regions next to each wall where the profile is significant begin to overlap, making it impossible to distinguish between isotropic and nematic phases.

Let us now turn to discuss the effect of confinement on smectic ordering. The value of the chemical potential corresponding to the bulk transition to the smectic phase (from the isotropic phase in the case $L/D=3.7$ and from the nematic phase in the other two cases) is represented in Fig. 2 by means of a dashed line. Lines representing first-order transitions end in critical points at low values of H and form triple points at larger values of H. The latter are what we call smectic *pockets*. If one of these continuous lines is crossed along a vertical path by increasing the chemical potential at constant pore width (dotted vertical arrows in Fig. 2), the system undergoes a first-order transition from a disordered (I or N depending on the value of L/D) phase, where the number density in the central region of the pore is weakly (or not at all) structured, to a smectic phase where well-structured peaks exist throughout the pore. This is a *capillary smectization* line. On the other hand, for fixed chemical potential well above the corresponding value for the bulk transition μ_{DS}^{coex}, the system undergoes a series of first-order layering transitions as the pore width H is varied and the boundaries of the pockets are crossed. These are *layering transitions*. Note that these transitions can also be obtained for fixed pore width by varying the chemical potential. Each *pocket* is associated with a smectic phase composed of n layers, and each layering transition involves two structures with numbers of layers differing by one unit. The above transitions can be characterized by suitably defined order parameters. A standard way to introduce order parameters for an inhomogeneous fluid confined into a pore is via density and orientational order adsorption parameters, Γ_ρ and Γ_η:

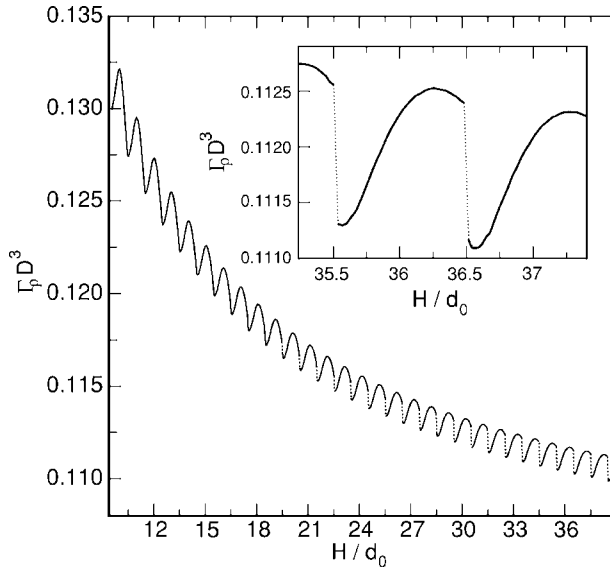$$\Gamma_\rho(\mu, H) = \int_0^H dz[\rho(z; \mu, H) - \rho_{coex}(\mu)],$$

FIG. 3. Density adsorption parameter Γ_ρ as a function of pore width H for elongation $L/D=5$ and chemical potential μ/kT $=21.70$. The inset shows enlarged area. Dotted lines indicate first-order layering transitions.

$$\Gamma_\eta(\mu,H) = \int_0^H dz\, \eta(z;\mu,H). \tag{9}$$

First-order phase transitions of the fluid in the pore are associated to discontinuous jumps of one (or both) of these parameters. In Fig. 3 the behavior of the density adsorption Γ_ρ as a function of pore width H is plotted for particle elongation $L/D=5$. The chemical potential, which is larger than that at which the bulk transition occurs, was chosen such that the first layering transitions are missed; for $H \gtrsim 19.5d_0$ a series of discontinuous changes in Γ_ρ occur, each corresponding to completion of a new smectic period, i.e., a layering transition. Here d_0 is the bulk smectic period at coexistence. In this case the discontinuity is negative; we will comment on this later.

The graph in Fig. 2, which contains the essential results of this work, shows how two (in principle unrelated) phenomena, i.e., layering and capillary condensation of a spatially ordered (such as the smectic) phase, are connected: the capillary smectization line, which oscillates as it tends to the bulk value μ_{DS}^{coex}, shows cusps, actually triple points, for pore widths H larger than some value, points at which high-order layering transitions terminate. For narrow pores the transitions associated with the two phenomena are even more intimately related, as they merge into a single transition line; as a consequence, regions of stability of structures that for wider pores were disconnected now become connected. These phenomena are associated with the strong commensuration effects arising from the periodicity of the smectic phase. We now turn to discuss the physical origin of the various features of these phase diagrams.

IV. CONNECTION TO WETTING BEHAVIOR

In the previous section we have presented the basic features of the phase diagrams schematically. These are common features in all phase diagrams. There are, however, specific features depending on the length-to-breadth ratio of the particles. For example, in the case of particles with low aspect ratio ($L/D=3.7$), the smectic pockets tend to appear at higher chemical potential as the pore width is increased, tending to μ_{IS}^{coex} from below and never crossing the line $\mu =\mu_{IS}^{coex}$. By contrast, in the other two cases (particles with larger aspect ratio), the smectic pockets show a nonmonotonic behavior: the capillary smectization line $\mu_{NS}(H)$ first occurs above the bulk value μ_{NS}^{coex}, then crosses this value, and finally tends to it as $H \to \infty$. In all cases there is a clear effect on smectization due to confinement.

The asymptotic behavior (when $H \to \infty$) of these capillary transition lines can again be rationalized in terms of the wetting properties of the system by means of the Kelvin equation. In this case we write

$$\Delta\mu_0(H) \equiv \mu_{DS}(H) - \mu_{DS}^{coex} = \frac{2(\gamma_{WS} - \gamma_{WD})}{(\rho_S - \rho_D)H},$$

$$H \to \infty, \quad D = N \text{ or } I, \tag{10}$$

where ρ_S and ρ_D are the number densities of the bulk smectic and disordered (N or I) phases, respectively. γ_{WD} stands for the wall-nematic or wall-isotropic surface tension (one or the other is involved depending on the value of L/D), and γ_{WS} is the wall-smectic surface tension. This equation is modified when elastic contributions to the smectic phase are taken into account [25]; we discuss this point later. For the moment, we use the Kelvin equation to obtain the "average" behavior of the transition line $\mu_{DS}(H)$. The sign of the second term in Eq. (10) gives the slope with which the capillary transitions tend to their bulk asymptotic values. Since $\rho_S > \rho_D$ this sign is controlled by the surface tension difference $\gamma_{WS} - \gamma_{WD}$. The relevant surface tensions can be calculated consistently within our DFT theory in semiinfinite geometry, and predictions of the asymptotic behavior can be made.

The calculation of the surface tension (excess grand potential, over bulk value for the same chemical potential and volume, per unit area) of a WS interface is somewhat problematic, since we need to place a boundary condition in the form of a bulk smectic profile at some distance from the wall and away from it. Ideally this condition should be at infinity since the elastic stress induced by the boundary condition is freed very slowly. In practice a collection of systems with different distances from the wall to the boundary condition can be set up, the equilibrium structure obtained for each, and the resulting excess grand potential per unit area minimized with respect to the distance of the boundary condition from the wall. An alternative approach, which avoids the need to deal with a boundary condition, is to place the smectic into different slitlike pores of varying width, and minimize the excess grand potential with respect to the width. The true surface tension γ_{WS} is obtained by subtracting the bulk grand potential from the grand potential of the film, dividing by a factor 2 and extrapolating to the limit $H \to \infty$. To insure bulk conditions at the center of the pore the grand-potential density and the layer spacing can be monitored and compared with their corresponding bulk values. The WD in-
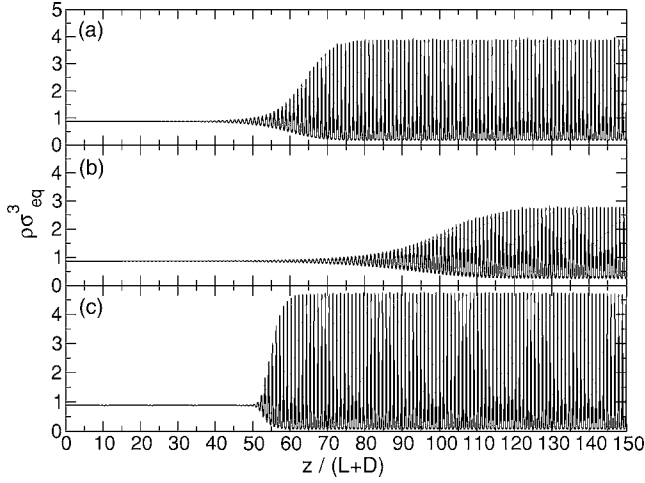
FIG. 4. Density profiles of the (a) (b) SN interface, and (c) SI interface. The first two cases correspond to the systems with L/D =6 and 5, respectively, whereas the other corresponds to the case L/D=3.7.

terfaces, by contrast, present no difficulties, and the surface tension γ_{WD} can be obtained in semiinfinite geometry, applying a uniform boundary condition. The calculation of γ_{DS} (which is not strictly necessary to apply the Kelvin equation, but is needed to obtain the wetting properties of the film) is, again, not easy. The reason is that it is not clear how to locate the Gibbs dividing surface and therefore there is some ambiguity in the calculation of excess surface quantities. The problem can be solved, however, by calculating the film tension of a freely suspended smectic film (in nematic or isotropic coexistence depending on the surface tension, γ_{NS} or γ_{IS}, to be calculated). The corresponding surface tension is half of the film tension in the limit of very thick films [38]. Figure 4 shows the DS profiles for the three aspect ratios considered (only half of the film is shown). Note that in the case L/D=5 the NS interface is very wide and correspondingly the surface tension is very low with respect to the two other cases [39]. Table I contains several results obtained for the different interfaces [40] along with other parameters and coexistence properties [41,42]. In all cases $\gamma_{WS} < \gamma_{WD}$ (i.e., the wall is preferentially wet by the smectic phase over the disordered phase), so that the prediction of the Kelvin equation is that the average capillary smectization line tends to the bulk value from below in the asymptotic limit (this is consistent with the behavior presented schematically in Fig. 2(a); in the other cases, (b) and (c), it implies a nonmono-

tonic behavior of the average capillary transition line). In any case, the value of the difference $\gamma_{WS} - \gamma_{WD}$ makes it clear that there is stronger wetting by smectic in the case L/D =3.7, and this fact explains the stronger smectization effect due to confinement observed in this case and shown by the fact that the smectic pockets are always below the horizontal line $\mu = \mu_{IS}^{coex}$.

Before continuing with our discussion on the phase diagrams, we briefly comment on the wetting behavior extracted from the data in Table I. This behavior is controlled by the value of the spreading coefficient S. In the case L/D=3.7 where, as already mentioned, the nematic phase is not stable, the relevant surface tensions are γ_{WS}, γ_{WI}, and γ_{SI}. In general we would have $\gamma_{WI} \leq \gamma_{WS} + \gamma_{SI}$, with the inequality corresponding to a partial wetting situation and the equality to complete wetting of the WI interface by the smectic phase. The data in Table I give a value for the spreading coefficient $S = \gamma_{WI} - \gamma_{WS} - \gamma_{SI} = 230 \times 10^{-5} kT/D^2 > 0$. This points to a nonequilibrium situation in our conjugate-gradient minimization, where the thickness of a smectic layer is increasing and the surface tension of the WI interface γ_{WI} is decreasing. The conjugate-gradient method employed in the minimization of the density functional is unable to reach the true equilibrium thickness within the computational time, since the thermodynamic force pushing the IS interface away from the wall is too weak. A more rigorous study based on the technique of the effective surface-tension-adsorption characteristic would be required [43], but we believe that, since the thickness of the smectic layer at the end of the minimization process is already large, we have a situation of complete wetting. In the case L/D=5 the relevant equation is $\gamma_{WN} \leq \gamma_{WS} + \gamma_{SN}$, which gives for the spreading coefficient $S = \gamma_{WN} - \gamma_{WS} - \gamma_{SN} = 7 \times 10^{-5} kT/D^2$. This is a small but again positive quantity. For the case L/D=6 the data are also consistent with a situation of complete wetting by smectic ($S = 11 \times 10^{-5} kT/D^2$). These conclusions should be taken with caution, since the accuracy of the different surface tensions are probably close to the values of the spreading coefficient obtained, at least for the cases L/D=5 and 6.

V. CONDITIONS FOR OCCURRENCE OF CONNECTED SMECTIC POCKETS

Now we turn to the question of how the phase behavior in the regime of narrow pores varies as a function of L/D. As discussed in Sec. III, when H is large there is a sequence of triple points where two smectic phases S_n and S_{n+1}, differing

TABLE I. Values of reduced chemical potential at bulk coexistence, $\mu_{DS}^{coex*} = \mu_{DS}^{coex}/kT$, reduced surface tensions γ^* (with $\gamma^* = \gamma D^2/kT$), spreading coefficient S^* (with $S^* = SD^2/kT$) of the different interfaces, coexistence densities in reduced units ($\rho^* = \rho D^3$), bulk smectic layer spacing d_0^* (with $d_0^* = d_0/D$), and reduced layer compressibility of the smectic phase, $B^* = BD^3/kT$, as a function of the length-to-breath ratio L/D. D is the particle breadth. The nature of the disordered phase is $D=I$ for L/D=3.7 and $D=N$ for L/D=5 and 6.

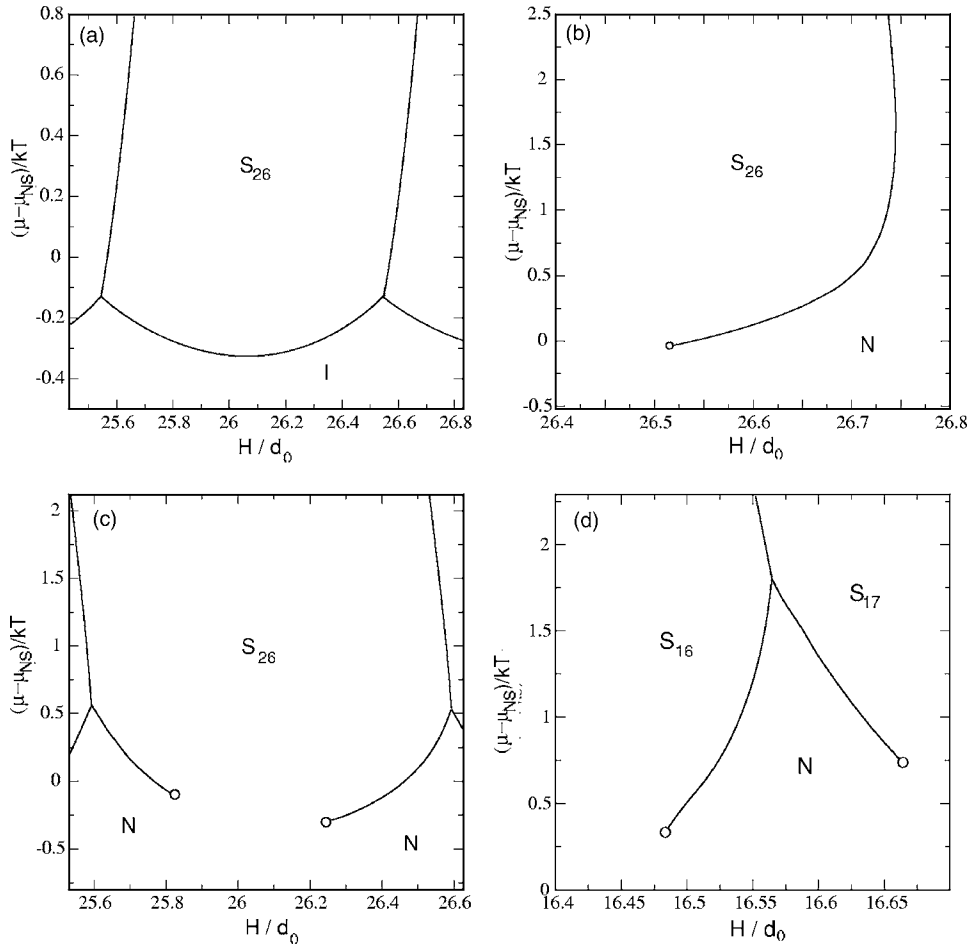| L/D	μ_{DS}^{coex*}	γ_{WS}^*	γ_{WD}^*	γ_{DS}^*	$10^5 \times S^*$	$\gamma_{WS}^* - \gamma_{WD}^*$	ρ_D^*	ρ_S^*	d_0^*	B^*
3.7	24.098	−4.2470	−4.1036	0.1411	230	−0.1434	0.1356	0.1466	4.784	8.85
5	21.636	−3.3785	−3.3692	0.0092	7	−0.0093	0.101	0.103	6.267	2.78
6	21.651	−3.3306	−3.2956	0.0349	11	−0.0350	0.086	0.089	7.416	5.64

FIG. 5. Phase diagrams of the confined system in the region corresponding to a few smectic layers. (a) $L/D=3.7$; (b) $L/D=5$; (c) and (d) $L/D=6$.

by one layer, and a disordered D phase (isotropic or nematic), may coexist in equilibrium. This structure is maintained as H increases. The triple points disappear for narrow pores, at some layer index n, and the smectic regions of n and $n-1$ layers become connected. There is a critical number of smectic layers n_c, which separates the regime of triple points from the regime where smectic regions become connected. Our DFT results for n_c (which are just estimates based on selective analyses of a few smectic pockets) exhibit a nonmonotonic behavior as a function of the length-to-breadth ratio: while for $L/D=3.7$ the critical number of layers is small ($n_c \simeq 10$), for $L/D=5$ it increases by an order of magnitude ($n_c \simeq 100$) while for $L/D=6$ it decreases again ($n_c \simeq 15$). Figures 5(a)–5(c) show results corresponding to the smectic *pocket* of 26 layers for the three values of L/D considered. In the first case ($L/D=3.7$) the system is in the regime of disconnected smectic regions. In the second case ($L/D=5$) the pockets have become completely connected via the appearance of a critical point in the N-S transition in the left region of the pocket [see schematic representation in Fig. 2(b)]; this we call *first scenario*. In the third case ($L/D=6$) pockets are connected via a *second scenario*, i.e., through the breaking of the N-S transition at the middle of the pocket and the appearance of two critical points. This creates lambda-shaped transition lines (schematically represented in Fig. 2), another example of which is shown in Fig. 5(d) for the case $L/D=6$. As one considers narrower pores the length of the

transition line ending in the critical point at the right decreases; although we have not verified this explicitly, we believe that this line eventually disappears, which would leave a single transition line of the shape shown in Fig. 5(b) [see schematic phase diagram in Fig. 2(c)].

Our density-functional calculations predict that in the first two cases, $L/D=3.7$ and 5, the pockets are broken via the first scenario, while in the case $L/D=6$ we have the second scenario. The reason for the different mechanisms has to do with the free energies involved between the nematic film and the compressed (leftmost region of pocket), S_n^c, stretched (rightmost region), S_n^s, or stress-free (intermediate region), S_n^{sf}, smectic films. The values of the free-energy barriers for the pairs of phases N-S_n^c, N-S_n^s, and N-S_n^{sf} gives an indication of which scenario may be applicable in each case, since the lesser the value of this difference the greater the possibility for the two phases to become connected. The height of the barriers is in turn related to the similarity between the structure of the nematic and smectic phases that coexist prior to breaking of the first-order coexistence line.

The nonmonotonic behavior of the critical number of layers n_c with L/D can be understood in terms of the balance between the cost in elastic free energy associated with stretching or compressing the smectic film by varying the value of H, keeping the number of layers constant, and the free-energy cost involved in introducing the disordered phase in the central region of the pore, $2\gamma_{DS}$ (since two new interfaces are added). This argument is valid provided a model

based on the assumption of abrupt interfaces can be made; since this assumption may not be strictly valid in some cases, the argument is to be taken only as qualitative. The elastic energy per unit area is proportional to the layer compressibility and, for a film with n smectic periods, can be estimated as [44]

$$\frac{B}{2H_n}\left(\frac{d_0}{2}\right)^2 = \frac{Bd_0}{8n}, \tag{11}$$

where $H_n \equiv nd_0$ [45] (this expression assumes the film to be compressed by half a period). We obtain $n_c \sim Bd_0/16\gamma_{DS}$ for the critical number of layers. Since B depends only weakly on L/D, but the surface tension of the DS interface is strongly dependent (see Table I) due to the different nature of the disordered phases involved [39], very different values of n_c are obtained: for the cases $L/D = 3.7$, 5, and 6 we have, respectively, $n_c \simeq 20$, 120, and 75; these numbers are in order-of-magnitude agreement with the results based on DFT calculations [42].

VI. ELASTIC EFFECTS AND CLAUSIUS-CLAPEYRON EQUATION

The shape of the pockets can be understood in terms of the elastic energy involved when the layers are compressed or expanded with respect to their bulk equilibrium configuration. When $H = H_n = nd_0$, where d_0 is the bulk smectic layer spacing, there is in principle no elastic energy stored, and the points $\mu_{DS}(H_n)$, with n a large integer, should tend monotonically to the chemical potential at bulk coexistence, following the prediction of the Kelvin equation at large H. The modification introduced in the Kelvin equation by the elastic contribution in a closely related physical system has been discussed in Ref. [25]. Equating the grand potentials per unit area of smectic and nematic (or isotropic) phases (with the latter augmented by the elastic contribution), assuming $\Delta\mu(H) = \mu(H) - \mu_{DS}^{coex}$ is small, we get

$$H(\omega_S^{coex} - \rho_S^{coex}\Delta\mu) + 2\gamma_{WS} + B\frac{(H-H_n)^2}{2H_n}$$
$$= H(\omega_D^{coex} - \rho_D^{coex}\Delta\mu) + 2\gamma_{WD}, \tag{12}$$

where ω^{coex} is the grand potential per unit volume of each phase. Since $\omega_S^{coex} = \omega_D^{coex}$, and letting $\Delta\rho_{coex} = \rho_S^{coex} - \rho_D^{coex}$, we obtain

$$\Delta\mu_n(H) = \Delta\mu_0(H) + \left(\frac{B}{2H_n\Delta\rho_{coex}}\right)\frac{(H-H_n)^2}{H}, \quad n \gg 1 \tag{13}$$

which is the modified Kelvin equation (MKE). The second term accounts for the elastic contribution, and corrects the Kelvin equation when film elasticity is important. For each value of n the possible values of H are within an interval about H_n, say $H = H_n \pm d_0/2$. Since the prefactor of the elastic contribution is positive, the MKE predicts that the capillary smectization line in each smectic period has a concave (approximately quadratic) shape. Also, it predicts that the line should be quite symmetrical, since $\Delta\mu_0(H)$ varies, within a
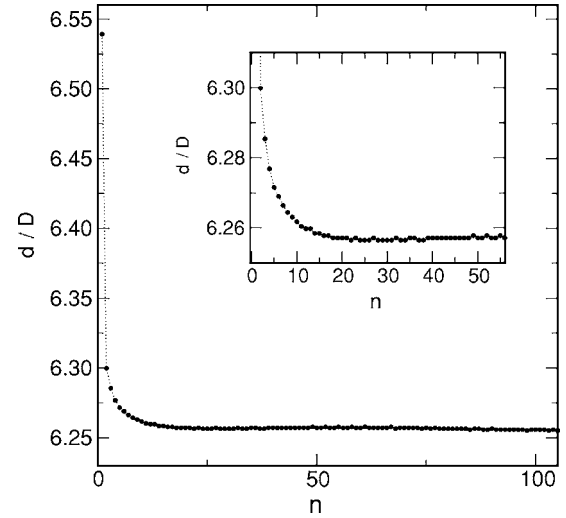

FIG. 6. Smectic layer spacing d for a smectic phase within a pore containing 210 layers (due to the symmetry of the profiles, only half of the layers are shown), and for a fluid with $L/D = 5$ and $\mu = 21.64kT$.

smectic period, only by a small amount ($\simeq c/n^2$, with n the layer index and c a constant which in the cases considered is in the interval $\simeq 1.5-5.5$) for high layer indices. This indeed agrees with the predictions of our DFT calculations, as will be described in the following.

Values for the constants B, $\Delta\rho_{coex}$, d_0, H_n and for the constants in $\Delta\mu_0(H)$ can be obtained from our DFT approximation and used in the MKE to obtain quantitative predictions on the shape of each pocket; in this way we can assess the validity of the MKE and its range of applicability. The first three constants pose no problem (see the Appendix for details). However, the calculation of H_n (i.e., the pore width for which there would not be any elastic stress stored in the system), which gives the location of the minimum, is not direct in DFT. It is not simply $H_n = nd_0$ for some value of n, since the layer spacing in the pore is far from uniform: the walls create a larger spacing between the first and the next layer (this is reasonable since the wall is hard) compared with the bulk value, and this misfit slowly relaxes via elastic forces away from the walls. Figure 6 shows this effect in some particular instance (in this case the pore width H is such that the layer spacing d as a function of layer index tends to the bulk value in the central region of the pore). Also, the bulk layer spacing may not even exist if the chemical potential is below that of the bulk N-S transition. In addition, the contribution $\Delta\mu_0(H)$ from the KE should be quantitative only in the asymptotic limit. In view of this, and in order to extract some information from the MKE, we have simply located the function given by Eq. (13) at the minimum given by the density-functional calculations (which implies fixing the value of the Kelvin term and choosing the appropriate value for H_n), used the computed value for B and plotted the resulting function of H; this is done in Fig. 7 for the case $L/D = 5$ and a high-index pocket ($n = 210$). The N-S transition is only approximately reproduced, which may be an indication that the asymptotic regime is still far from being reached (note that, apart from the problem of elastic
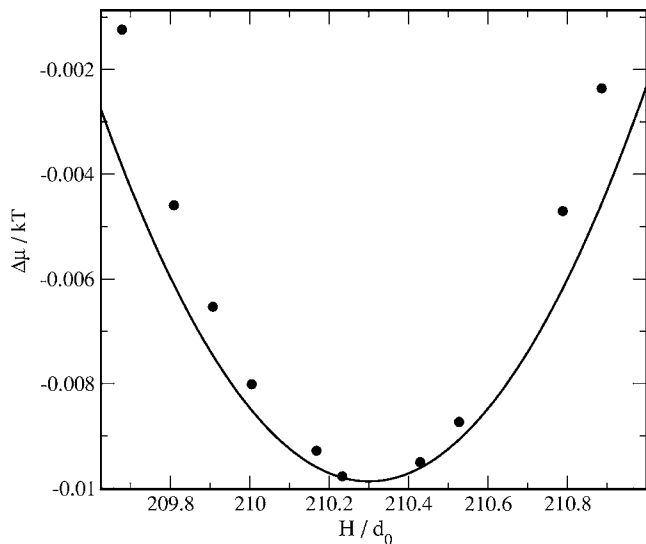
FIG. 7. N-S transition line in the pocket corresponding to 210 smectic layers. Solid lines: prediction of modified Kelvin equation (see text for an explanation); symbols: present density-functional calculations.

contributions mentioned above, the effective-interface model used to derive the Kelvin equation, which assumes perfectly well-developed interfaces, may not be entirely valid even for very thick films due to the slow relaxation of the structure away from the walls).

Finally, the Clausis-Clapeyron equation for two arbitrary coexisting films 1 and 2 can be obtained and used to discuss the different slopes of the first-order transition lines in the phase diagram. We have

$$\left(\frac{\partial \mu}{\partial H}\right)_T = \frac{f_1 - f_2}{\Gamma_2 - \Gamma_1}, \qquad (14)$$

where f_1 and f_2 are the solvation (or disjoining) forces (excess over bulk pressure at fixed chemical potential and surface area) of the two films, and Γ_1, Γ_2 their density adsorptions. If this is applied to the D-S_n transitions, given that $\Gamma_{S_n} > \Gamma_N$, the interval with negative slope (left of the minimum) in each pocket is associated with $f_N < f_{S_n}$, whereas at the right of the minimum, where the slope is positive, we must have $f_N > f_{S_n}$. These conclusions are intuitively clear: for example, in the latter case, the smectic film is swollen with respect to the natural (bulk) layer spacing and a large attraction between the two plates results; in the case of the nematic f_N is also negative but small in absolute value. In the sector at left f_{S_n} is positive and large, while f_N is again negative but small in absolute value. The slope of the layering transitions in the μ-H phase diagrams varies depending on the particle elongation (it can also depend on the order of the layering transition and the value of the chemical potential), and can also be discussed using the above equation. In this case the equation involves f_{S_n} and $f_{S_{n+1}}$, the solvation forces of the two smectic films, and Γ_{S_n} and $\Gamma_{S_{n+1}}$, their adsorptions. Since now $f_{S_{n+1}} > f_{S_n}$ (introducing an additional layer into an n-layer, swollen smectic phase with $f_{S_n} < 0$, i.e., attractive

solvation force, at fixed pore width adds a pushing force coming from the $n+1$ (shrinked) layers, increasing the solvation force and making it positive, $f_{n+1} > 0$, i.e., repulsive solvation force), the change of slope is linked to a change in the sign of $\Gamma_{S_n} - \Gamma_{S_{n+1}}$. In the case depicted in Fig. 5(a) it can be shown that there is a negative density jump as the layering transitions $S_{25} \rightarrow S_{26}$ or $S_{26} \rightarrow S_{27}$ are crossed at constant chemical potential, and the slope of $\mu(H)$ is positive. In the case of Fig. 5(c) the opposite is true. There are cases where the two situations occur [see, e.g., Fig. 5(b)]. In these cases the two coexistence densities are equal, the slope of $\mu(H)$ goes to infinity, and the layering transition line becomes vertical.

VII. CONCLUSIONS

In this work we have analyzed the structure and phase behavior of a liquid crystal model confined in a slitlike pore. The model, the hard-spherocylinder model, is analyzed theoretically using a sophisticated density-functional approximation specially suited to dealt with highly inhomogeneous fluids, and modified to include orientational order. The fluid is highly structured next to the walls confining the fluid, and different confined phases are found, which can be associated with confined isotropic, nematic, and smectic phases. As expected, strong commensuration effects arise in the fluid, due to commensuration between the equilibrium (bulk) layer spacing of the layers and the pore width. This brings about a variety of interesting phase behaviors, with a complicated structure of first-order phase transitions separating different phases, but also critical points beyond which confined phases are connected. The topology of the phase diagram has been analyzed with respect to aspect ratio. The topology is similar, containing layering transitions, capillary smectization transitions and, when the nematic phase can be stabilized at bulk, capillary nematization transitions. The first two features are intimately related to each other and, for very narrow pores, the two phenomena become a single one. The various aspects of the phase diagrams have been connected to the wetting behavior and the Clausius-Clapeyron equation.

Two questions (among many others) that remain to be addressed are the following: (i) How confined crystalline phases enter the picture. The bulk samples possess crystalline phases at higher chemical potentials. These phases will undergo layering and capillary transitions similar to those predicted for the smectic films. A more sophisticated theory will be required to tackle this problem. (ii) Different surface affinities for the smectic phase will certainly modify some of the phenomena presented in this work. For example, conditions for which the smectic phase partially wets the plates may lead to a qualitatively different global approach to bulk or even to a total suppression of capillary smectization and/or the layering transitions. These aspects will be studied in future work.

ACKNOWLEDGMENTS

APPENDIX: THEORETICAL MODEL AND IMPLEMENTATION

In this Appendix we provide some details on the actual implementation of the density-functional theory for the problem at hand, and give some numerical details. In view of the translational symmetry in the xy plane of our problem, the one-particle distribution function depends only on the normal distance from one of the walls z. The ideal free energy can then be written as

$$\frac{F_{id}[\rho]}{kTA} = \int_0^H dz\rho(z)\left\{\ln\left[\frac{\rho(z)\Lambda^3}{4\pi}\right] - 1\right\} - \int_0^H dz\rho(z)S_{\text{rot}}(z),$$

(A1)

where A is the transverse area of the system and H is the pore width. The local rotational entropy per particle is given by

$$S_{\text{rot}}(z) = -\int d\mathbf{\Omega} f(z,\mathbf{\Omega})\ln[4\pi f(\mathbf{z},\mathbf{\Omega})].$$

(A2)

The other contribution to the free energy is the excess contribution $F_{ex}[\rho]$, which accounts for the effect of interactions, both intrinsic (interactions between fluid particles) and also extrinsic (interactions between particles and pore walls). Since we are interested in highly nonuniform systems, our approximation needs to be nonlocal in order to account for the expected density profile structures. We use the Somoza-Tarazona density-functional approximation, a generalized decoupling approximation for anisotropic hard bodies [34,46]. The intrinsic part of the excess free energy is given in Eq. (2). In that expression, $\Psi_{\text{ex}}^{\text{PHE}}(\rho)$ is the excess free energy of an effective system of parallel hard ellipsoids (which is known since its thermodynamics can be exactly mapped onto that of a system of hard spheres), $V_{\text{exc}}(\mathbf{r}-\mathbf{r}',\mathbf{\Omega},\mathbf{\Omega}')$ is the (negative) Mayer function of two spherocylinders, $\bar{\rho}(\mathbf{r})$ is an averaged density which takes into account the structure of the system in the neighborhood of $\mathbf{r}$ in an appropriate manner (we shall briefly discuss this point below), and $\bar{\rho}_{\text{PHE}}(\mathbf{r})$ is the local averaged density of a system of parallel hard ellipsoids, defined by the following equation [33]:

$$\bar{\rho}_{\text{PHE}}(\mathbf{r}) = \int d\mathbf{r}'\rho(\mathbf{r}')V_{\text{exc}}^{\text{PHE}}(\mathbf{r} - \mathbf{r}'),$$

(A3)

where $V_{\text{exc}}^{\text{PHE}}(\mathbf{r})$ is the (negative) Mayer function of two parallel hard ellipsoids. Let $\sigma_{\parallel}$ and $\sigma_{\perp}$ be the length and breadth of the hard ellipsoids, respectively. Since the system of parallel hard ellipsoids is a sort of auxiliary system in this theoretical model, the real one being a system of hard spherocylinders, the question of how to choose $\sigma_{\parallel}$ and $\sigma_{\perp}$ for given spherocylinder has to be solved in order to proceed. In the

original formulation of the theory, Somoza and Tarazona proposed a recipe based on equating the inertia tensors of both particles [34,46]. A simpler choice is that of Velasco *et al.* [33] who used the criteria of equal molecular volume v and equal length-to-breadth ratio. These two conditions lead to the relations

$$\frac{\sigma_{\parallel}}{\sigma_{\text{eq}}} = \left(1 + \frac{L}{D}\right)^{2/3}, \quad \frac{\sigma_{\perp}}{\sigma_{\text{eq}}} = \left(1 + \frac{L}{D}\right)^{-1/3}, \quad \text{(A4)}$$

with L and D being the length and breadth of the spherocylinder, respectively, and $\sigma_{\text{eq}} \equiv (\sigma_{\perp}^2\sigma_{\parallel})^{1/3}$ is the diameter of the equivalent hard spheres (both the spheres and the ellipsoids have the same volume and therefore both systems have the same packing fraction). A system of such hard spheres can be easily shown to be thermodynamically equivalent to the reference system of parallel hard ellipsoids by means of a simple change of scale in one direction. In particular, nonlocal weighted density approximations for nonuniform hard-sphere systems can be easily extended to deal with the reference system of parallel hard ellipsoids [47]. In this way, $\Psi_{\text{ex}}^{\text{PHE}}(\rho)$ will be given by the excess free energy per particle of a uniform system of hard spheres of diameter σ_{eq} (accurately obtained from the well known Carnahan-Starling fit), and the weighted density can be expressed in terms of three average local densities $\rho_n(\mathbf{r})$, $n = 0, 1, 2$, given by

$$\rho_n(\mathbf{r}) = \int d\mathbf{t}\omega_n(|\mathbf{t}|)\rho(\mathbf{r} + \tilde{\sigma} \cdot \mathbf{t}),$$

(A5)

where $\tilde{\sigma}$ is a diagonal tensor in the reference frame defined by the director (with components $\sigma_{\parallel}$ and $\sigma_{\perp}$ along the axis parallel an perpendicular to the director, respectively). The expressions for the three weighting functions $\omega_n(r)$ can be found in the original work of Tarazona [35]. In our application, given that the spatial dependence in only along the z direction, it can be easily shown [33] that $\bar{\rho}_{\text{PHE}}(z) = \frac{4\pi}{3}\sigma_{eq}^3\bar{\rho}_0(z)$. On the other hand, the factor $\int d\mathbf{\Omega}\rho(\mathbf{r},\mathbf{\Omega})\int\int d\mathbf{r}'d\mathbf{\Omega}'\rho(\mathbf{r}',\mathbf{\Omega}')V_{\text{exc}}(\mathbf{r}-\mathbf{r}',\mathbf{\Omega},\mathbf{\Omega}')$ in Eq. (2) can be rewritten, using again $\rho(\mathbf{r},\mathbf{\Omega}) \equiv \rho(z,\mathbf{\Omega}) = \rho(z)f(z,\mathbf{\Omega})$, in terms of an effective potential ξ which is a functional of the orientational distribution function,

$$\int d\mathbf{\Omega}\rho(\mathbf{r},\mathbf{\Omega})\int\int d\mathbf{R}'d\mathbf{\Omega}'\rho(\mathbf{r}',\mathbf{\Omega}')V_{\text{exc}}(\mathbf{r} - \mathbf{r}',\mathbf{\Omega},\mathbf{\Omega}')$$

$$= \rho(z)\rho(z')\xi(z,z';[f]),$$

(A6)

with

$$\xi(z,z';[f]) \equiv \int d\mathbf{\Omega}\int d\mathbf{\Omega}'f(z,\mathbf{\Omega})f(z',\mathbf{\Omega}')$$

$$\times \int d\mathbf{R}'V_{\text{exc}}(z - z',\mathbf{R} - \mathbf{R}',\mathbf{\Omega},\mathbf{\Omega}') \quad \text{(A7)}$$

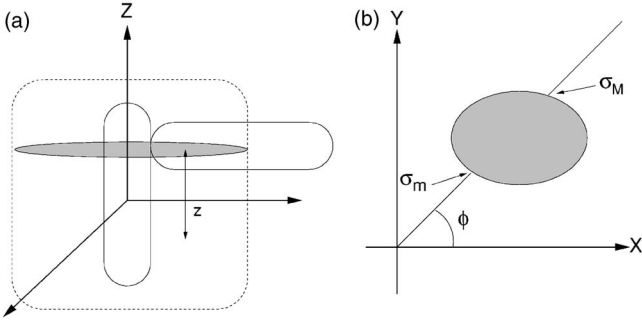and $\mathbf{R} = (x,y)$. The excess free energy then becomes

FIG. 8. (a) Schematic representation of the excluded volume of two HSCs (dashed line) and the excluded area (shaded region). (b) Graphical representation of σ_m and σ_M.

$$F_{ex}[\rho] = A \int dz \frac{\Psi_{ex}^{PHE}(\bar{\rho}(z))}{\bar{\rho}_{PHE}(z)} \rho(z) \int dz' \rho(z') \xi(z,z';[f]),$$

(A8)

where A is the system area. Using Eqs. (3) and (4) it is not difficult to show that there exists a one-to-one relationship between the values of the order parameters $\eta(z)$ and $\eta(z')$, and the effective potential $\xi(z,z')$. The same is true for the rotational entropy $S_{rot}(z)$ [33,48]. Therefore we can omit the orientational distribution function and use the profiles $\rho(z)$ and $\eta(z)$ to determine the equilibrium configuration. This fact allows us, in our practical implementation of this approximation, to calculate values for $\xi(z,\eta,\eta')$ and $S_{rot}(\eta)$ only once. These data can be stored in lookup tables and interpolated as needed. The central problem to evaluate the effective potential is the calculation of the spatial integral over $\mathbf{R}'$, which is the area of a planar section, perpendicular to the $\mathbf{z}$ axis, of the excluded volume of two spherocylinders with orientations $\mathbf{\Omega}$ and $\mathbf{\Omega}'$, at a distance z form its center, see Fig. 8(a). In previous work [31,33] a Fourier-series representation inspired by the work in Ref. [49] was used.

In Ref. [23] and in the present work we used an alternative method, originally proposed by Cinacchi [50], which improves the efficiency and also the accuracy of the calculation. In this method, we write the excluded area using polar coordinates in the xy plane as

$$A_{exc}(z,\mathbf{\Omega},\mathbf{\Omega}') \equiv \int d\mathbf{R}' V_{exc}(z,\mathbf{R}-\mathbf{R}',\mathbf{\Omega},\mathbf{\Omega}')$$

$$= \int_0^{2\pi} d\phi \int_{\sigma_m}^{\sigma_M} r dr$$

$$= \frac{1}{2} \int_0^{2\pi} d\phi \{\sigma_M^2(\phi) - \sigma_m^2(\phi)\}, \quad (A9)$$

where σ_m and σ_M are functions of ϕ, z, $\mathbf{\Omega}$, and $\mathbf{\Omega}'$. For fixed values of ϕ, z, $\mathbf{\Omega}$ and $\mathbf{\Omega}'$, σ_m and σ_M are the distances to the main axis of the central particle defining the overlap region between the two HSCs (see Fig. 8), and are calculated numerically using the overlap criterion between two particles. The integral over ϕ in Eq. (A9) were calculated using the

trapezoidal rule with 10^3 points in the interval $[0,2\pi]$, and the distances σ_m and σ_M were obtained with an accuracy of $10^{-7}(L+D)$. This method to evaluate $A_{exc}(z,\mathbf{\Omega},\mathbf{\Omega}')$ improves the quality of the numerical minimization, and is feasible in uniaxial systems, where η is the only nonvanishing orientational order parameter [24]; when more order parameters are needed to describe the system, as in the case of biaxial system, the lookup table may depend on too many variables to make the method practical. The potential $\xi(z,z';[f])$ is obtained from Eq. (A7); angular integrals $\int d\hat{\mathbf{\Omega}} \int d\hat{\mathbf{\Omega}}' \rightarrow 2\pi \int d\theta \sin \theta \int d\theta' \sin \theta' \int d\phi$ are done by Gaussian quadrature in all three angular variables, using 46 roots in each variable. This procedure produces a table with entries (z,η,η'), which was constructed with a step $\Delta \eta = 0.01$ in the domain $[-0.40,0.99] \times [-0.40,0.99]$, and a spatial step equal to that used to evaluate the spatial integrals (see later). The table for the orientational entropy was constructed in a similar way.

To end we provide some numerical details on the evaluation of the free energy and its minimization. Integrals over z and z' [see Eqs. (A2) and (A8)] were computed using the trapezoidal rule with step size $\Delta z = 0.05$ in the cases $L/D = 5$ and 6, and $\Delta z = 0.03$ for $L/D = 3.7$. Checks were made with smaller sizes to assess the numerical accuracy. The functional was minimized using a conjugate-gradient method. The criterion for equilibration (converged profiles) is based on the value of the modulus of the gradient per variable, g. The criterion used was $g < 10^{-6}$ (in units where $kT = 1$, $D = 1$), except in the calculations of wetting properties where we used $g < 10^{-7}$. The number of iterations necessary for a profile to converge depends very much on the nature of the phase, the pore width, the initial profile, and the thermodynamic conditions, among others. Typically, an isotropic profile with a bad initial guess converges quite quickly (in about 100–200 iterations), whereas a smectic profile with a bad initial profile requires numbers in excess of 4000 iterations. Once a smectic profile is equilibrated, a profile corresponding to new thermodynamic conditions close to the previous ones normally require only 100–200 iterations.

Bulk properties were calculated using the same procedure, except that periodic boundary conditions were employed. For the smectic phase slabs containing about 20 layers were used, minimizing with respect to $\rho(z)$, $\eta(z)$, and d at fixed number of layers, volume, and chemical potential [nematic and isotropic phases were calculated in slabs of the similar width, minimizing with respect to $\rho(z) = \rho_0$—the mean density—and, in the case of the nematic, also with respect to $\eta(z) = \eta_0$]. Coexistence is calculated by equating the grand potentials (equal-pressure criterion) of the two phases involved at the same chemical potential. The layer compressibility is calculated from

$$B = \frac{1}{V}\left(\frac{\partial^2 \Omega}{\partial \lambda^2}\right)_{\lambda=0} = d_0^2 \left(\frac{\partial^2 \omega}{\partial d^2}\right)_{d_0}, \quad (A10)$$

where λ is a scale factor ("strain tensor") relating the distorted and undistorted smectic: $z' = \lambda z$ or $d = \lambda d_0$. The derivative is computed at fixed μ, V and evaluated at equilibrium.

[1] B. Jérôme, Rep. Prog. Phys. **54**, 391 (1990).

[2] T. J. Sluckin and A. Poniewierski, in *Fluid Interfacial Phenomena*, edited by C. A. Croxton (Wiley, London, 1986), p. 215.

[3] *Liquid Crystals: Applications and Uses*, edited by B. Badahur (Word Scientific, Singapore, 1990), Vol. 1.

[4] G. Vertogen and W. H. de Jeu, *Thermotropic Liquid Crystals* (Springer-Verlag, New York, 1988).

[5] See, e.g., D. Cleaver, S. Kralj, T. J. Sluckin, and M. P. Allen, *Liquid Crystals in Complex Geometries Formed by Polymer and Porous Networks* (Taylor and Francis, London, 1996); T. Bellini, L. Radzihovsky, J. Toner, and N. A. Clark, Science **294**, 1074 (2001).

[6] P. I. C. Teixeira, Phys. Rev. E **55**, 2876 (1997); R. van Roij, M. Dijkstra, and R. Evans, Europhys. Lett. **49**, 350 (2000); I. Rodriguez-Ponce, J. M. Romero-Enrique, E. Velasco, L. Mederos, and L. F. Rull, J. Phys.: Condens. Matter **12**, A363 (2000); A. Chrzanowska, P. I. C. Teixeira, H. Ehrentraut, and D. J. Cleaver, *ibid.* **13**, 4715 (2001); I. Rodriguez-Ponce, J. M. Romero-Enrique, and L. F. Rull, Phys. Rev. E **64**, 051704 (2001).

[7] M. P. Allen, J. Chem. Phys. **112**, 5447 (2000); J. Quintana, E. C. Poire, H. Dominguez, and J. Alejandre, Mol. Phys. **100**, 2597 (2002).

[8] T. Gruhn and M. Schoen, J. Chem. Phys. **108**, 9124 (1998).

[9] H. Steuer, S. Hess, and M. Schoen, Phys. Rev. E **69**, 031708 (2004).

[10] P. G. de Gennes, Langmuir **6**, 1448 (1990).

[11] Z. Kutnjak, S. Kralj, G. Lahajnar, and S. Zumer, Phys. Rev. E **70**, 051703 (2004).

[12] R. E. Webster, N. J. Mottram, and D. J. Cleaver, Phys. Rev. E **68**, 021706 (2003).

[13] K. Kocevar and I. Musevic, Phys. Rev. E **65**, 021703 (2002).

[14] L. Wu, B. Zhou, C. W. Garland, T. Bellini, and D. W. Schaefer, Phys. Rev. E **51**, 2157 (1995).

[15] N. A. Clark, T. Bellini, R. M. Malzbender, B. N. Thomas, A. G. Rappaport, C. D. Muzny, D. W. Schaefer, and L. Hrubesh, Phys. Rev. Lett. **71**, 3505 (1993).

[16] Z. Kutnjak, S. Kralj, G. Lahajnar, and S. Zumer, Phys. Rev. E **68**, 021705 (2003).

[17] L. D. Gelb, K. E. Gubbins, R. Radhakrishnan, and M. Sliwinska-Bartkowiak, Rep. Prog. Phys. **62**, 1573 (1999).

[18] P. C. Ball and R. Evans, J. Chem. Phys. **89**, 4412 (1988).

[19] G. Navascués and P. Tarazona, Mol. Phys. **62**, 497 (1987).

[20] P. Sheng, Phys. Rev. Lett. **37**, 1059 (1976); Phys. Rev. A **26**, 1610 (1982).

[21] A. Poniewierski and T. J. Sluckin, Liq. Cryst. **2**, 281 (1987).

[22] K. Kocevar, A. Borstnik, I. Musevic, and S. Zumer, Phys. Rev. Lett. **86**, 5914 (2001), and references therein.

[23] D. de las Heras, E. Velasco, and L. Mederos, J. Chem. Phys. **120**, 4949 (2004).

[24] D. de las Heras, E. Velasco, and L. Mederos, Phys. Rev. Lett. **94**, 017801 (2005).

[25] V. Babin, A. Ciach, and M. Tasinkevych, J. Chem. Phys. **114**, 9585 (2001).

[26] M. Tasinkevych and A. Ciach, Phys. Rev. E **72**, 061704 (2005).

[27] T. Geisinger, M. Muller, and K. Binder, J. Chem. Phys. **111**, 5241 (1999).

[28] L. Onsager, Ann. N.Y. Acad. Sci. **51**, 627 (1949).

[29] J. D. Parsons, J. Chem. Phys. **19**, 1225 (1979); S. D. Lee, *ibid.* **87**, 4972 (1987).

[30] R. Holyst and A. Poniewierski, Phys. Rev. A **38**, 1527 (1988).

[31] D. de las Heras, L. Mederos, and E. Velasco, Phys. Rev. E **68**, 031709 (2003).

[32] D. L. Cheung and F. Schmid, J. Chem. Phys. **120**, 9185 (2004).

[33] E. Velasco, L. Mederos, and D. E. Sullivan, Phys. Rev. E **62**, 3708 (2000).

[34] A. M. Somoza and P. Tarazona, Phys. Rev. Lett. **61**, 2566 (1988).

[35] P. Tarazona, Phys. Rev. A **31**, 2672 (1985).

[36] J. A. C. Veerman and D. Frenkel, Phys. Rev. A **41**, 3237 (1990).

[37] P. Bolhuis and D. Frenkel, J. Chem. Phys. **106**, 666 (1997).

[38] Y. Martinez, A. M. Somoza, L. Mederos, and D. E. Sullivan, Phys. Rev. E **53**, 2466 (1996).

[39] The smectic-isotropic interface is much more abrupt than the smectic-nematic interface, due to the larger density and order-parameter jumps at coexistence.

[40] Note that surface tensions of the wall-fluid interfaces may be negative since the walls are represented by inert substrates.

[41] Values for the coexistence densities differ slightly from those reported in Ref. [33] due to differences in the numerical implementation of the model.

[42] Note that the value of B reported in Ref. [24] for the case $L/D=5$ is incorrect.

[43] P. Tarazona and R. Evans, Mol. Phys. **48**, 799 (1983).

[44] This can be obtained from the elastic-theory expression $F_{\text{elas}} =(B/2)\int d\mathbf{r}(\partial u/\partial z)^2$; writing the displacement field as $u=\lambda z$, which implies $H=H_n(1+\lambda)$ for the pore width of the distorted smectic, we get a free energy per unit area $(B/2)(H-H_n)^2/H_n$.

[45] To estimate the elastic energy we assume that the smectic is compressed by an amount $d_0/2$. The elastic free energy per unit area of a film with $n-1$ layers, stretched by the same amount, is always less than that for an n-layer film, so that we can be sure that the pocket will be broken at the left boundary of the pocket. Using the same argument, we can predict that the pocket will never break in the region where the elastic film is small (central region of the pocket).

[46] A. M. Somoza and P. Tarazona, Phys. Rev. A **41**, 965 (1990).

[47] L. Mederos and D. E. Sullivan, Phys. Rev. A **39**, 854 (1989).

[48] E. Velasco, L. Mederos, and T. J. Sluckin, Liq. Cryst. **20**, 399 (1996).

[49] A. Poniewierski and T. J. Sluckin, Phys. Rev. A **43**, 6837 (1991).

[50] G. Cinacchi (private communication).